

# Liquid microlenses with adjustable focusing and beam steering for single cell optogenetics

S. R. Berry<sup>1\*</sup>, S. M. Redmond<sup>1</sup>, P. D. Robinson<sup>1</sup>, T. A. Thorsen<sup>1</sup>, M. Rothschild<sup>1</sup>, and E. S. Boyden<sup>2</sup>

1. MIT Lincoln Laboratory, Lexington, MA, USA

2. Department of Biological Engineering and Brain and Cognitive Sciences, MIT, Cambridge, MA, USA

\*Corresponding author: sberry@ll.mit.edu

**Abstract:** Two-dimensional numerical simulations were performed to guide the design of micron-scale liquid lenses that combine both adjustable focus and beam steering in a single optical element. The liquid microlens is formed by the interface between two immiscible liquids, having different indexes of refraction, contained in a conically tapered lens cavity. Adjustable focus and beam steering is achieved by controlling the curvature of the liquid-liquid interface through electrowetting. Changes in the interface shape as a function of voltage were modeled using the two-phase flow, level set method. Simulations were conducted for different cavity taper angles and voltage conditions. The interface profiles were then used to determine focal ranges and beam steering angles.

**Keywords:** Optofluidics, liquid lenses, optogenetics, electrowetting.

## 1.0 Introduction

Optogenetics consists of the selective photoexcitation of neurons, genetically modified to express photosensitive membrane proteins (opsins) [1-3]. Upon excitation, these opsins react by transporting ions into or out of neurons to control their electric activity. In optogenetics research, it is highly desirable to have a method that can deliver light and excite individual neurons in the brain in a controllable and single cell manner. Our eventual aim is to develop an implantable optical probe that has active focusing and beam steering placed at the end that will enable light delivery from an external laser source to individual neurons.

To target a volume containing ~100,000 neuron cell bodies would require a microlens system to have a focal range of 0.1 – 1 mm with the ability to simultaneously steer over  $\pm 5^\circ$ , plus be able to focus light down to a spot size of ~10  $\mu\text{m}$ . In addition, the microlens system has to be small, ideally <300  $\mu\text{m}$  in order to minimize cell damage during insertion. Working toward this goal, we are developing liquid

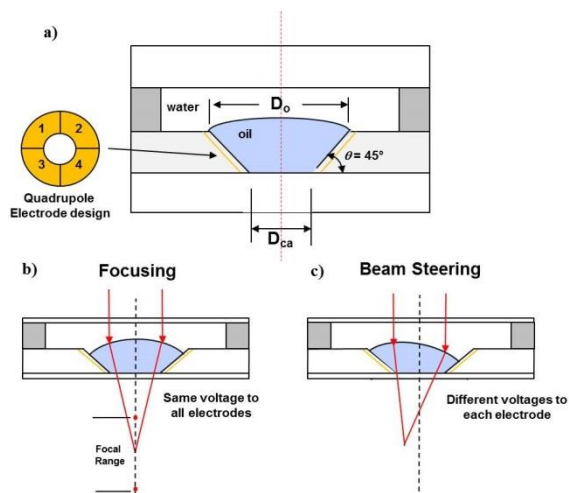


**Figure 1.** a) Liquid microlens design that combines both active focusing and steering by controlling the interface formed between two immiscible liquids.  $D_o$  is the lens diameter and  $D_{ca}$  is the clear aperture diameter. The liquid interface is contained within a conical taper that has a series of patterned metal electrodes along the sidewall. b) Variable focusing along the optical path will occur when the same potential is applied to all the electrodes. c) Beam steering will occur when different potentials are applied to each electrode pair.

microlenses on the order of 10's of microns in size with active electronics that enable both simultaneous focusing and beam steering in a single optical element.

In this design, the liquid microlens is formed by the interface between two immiscible liquids. A non-polar solvent (oil) is contained in a conically tapered lens cavity that is etched into a fused silica substrate and is surrounded by an aqueous phase (water) as shown in Fig. 1. Since the index of refraction for oils are typically greater than the index of refraction of water, variable focusing can be achieved by controlling the shape of the water-oil interface. To effectively focus and steer the light simultaneously, the liquid interface also needs to piston, i.e. tilt. This accomplished as a result of the tapered geometry which will allow the liquid-liquid interface to tilt, and still maintain a spherical profile.

Interdigitated metal electrodes are patterned along the taper sidewalls to electrically control the liquid-liquid interface through a phenomenon known as electrowetting [4]. Electrowetting has been used in the past for tunable optofluidic lenses [5-7]. The liquid lens focuses along the optical axis when the same voltage is applied to all the electrodes (Fig. 1b). Beam steering is accomplished as a result of applying different voltages to different electrodes (Fig. 1c). Details of the microlens design, fabrication process, and performance results can be found in [8]. The emphasis of this paper is on the numerical modeling that was used to guide the liquid microlens design.

To determine the appropriate liquid microlens size, taper angle, and taper depth, two-dimensional numerical simulations based on laminar, two-phase flow were performed. The equilibrium shape of the liquid-liquid interface was determined as a function of lens cavity taper geometry and applied voltages using the level-set method [9] in the CFD module in COMSOL Multiphysics® v5.2a. The profile shapes of the liquid-liquid interface were then used in analytical models to determine the focal range and beam steering angles for different size lenses and geometries.

## 2.0 Two-Phase Flow Modeling

In COMSOL Multiphysics® v5.2a there are three different numerical methods to simulate two-phase flow: level-set, phase-field, and moving mesh methods. All these methods allow for a moving fluid interface to be tracked, both spatially and temporally. The level-set and phase-field methods use a fixed background mesh to track the interface location. This is done by solving an additional transport equation along with the Navier-Stokes and continuity equations. In general, the phase-field method is more accurate than the level-set method because more physics surrounding the flow behavior are being solved [10]. However the phase-field method is computationally expensive. In this work, the level-set method was chosen since we are only after the mean position of the liquid lens profile and not the fine details of the flow field.

The level-set method uses a level-set contour function  $\phi = 0.5$  to define the fluid-fluid interface, where  $\phi = 0$  for fluid 1, and  $\phi = 1$  for fluid 2. Near the interface,  $\phi$  goes smoothly from 0 to 1 in a transition layer roughly equivalent to half the element size which the interface passes through. The numerical details of this method can be found in [9-11] and are reproduced in Appendix A as it pertains to this work.

The level-set method simulation procedure requires two consecutive computations. First a smooth initial solution is run to calculate the level-set

function. This determines the location of the fluid interface and defines the fluid domains. Next, using the initial solution, time-dependent simulations of the fluid motion are started.

## 3.0 Liquid Microlens Numerical Model Set-Up

The physics selected in COMSOL for the liquid microlens model is: 2D→Fluid Flow→ Multiphase Flow→Laminar Two-Phase Flow, Level Set → Level Set. The level-set method requires a phase initialization and time-dependent study step which is accomplished using the preset study: Transient with Phase Initialization.

Figure 2 shows an example of the liquid microlens geometry and boundary conditions used in the simulations. The geometry is defined by the taper angle  $\alpha$ , the taper cavity height  $h$ , and the clear aperture diameter  $D_{ca}$ . The geometry was created so that two geometric domains were formed and assigned material properties corresponding to the liquids used in this microlens design, which were deionized water (DI) and dodecane oil. In addition, the level-set function was assigned for each domain,  $\phi = 0$  for the water phase (fluid 1) and  $\phi = 1$  for the oil phase (fluid 2). The boundary interface between the domains was located approximately where the initial liquid-liquid interface would reside, near the top of the taper.

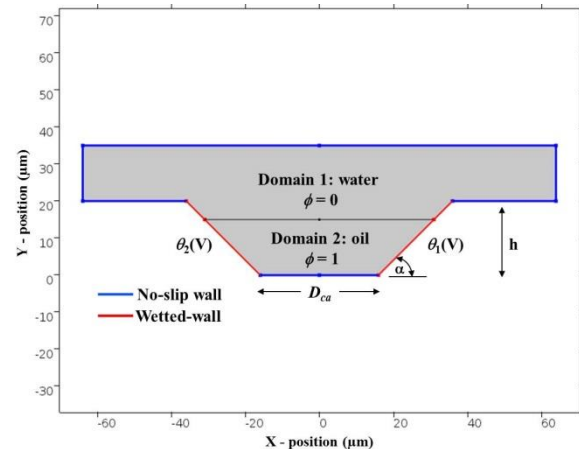


**Figure 2.** Boundary conditions used for the liquid microlens numerical model.

A no-slip wall boundary condition was used for all the exterior walls except for walls that form the conical taper. The boundary conditions for the taper sidewalls were set as wetted-walls. For this type of boundary condition, the contact angle that the fluid interface makes with the wall is specified and is defined as the angle from the wall to the interface

through fluid 2. In electrowetting, the surface energy of an interface is modified by the application of a voltage. This results in a change in contact angle for the case of a liquid drop on a solid electrode, separated by a thin dielectric. The change in contact angle can be accurately predicted from the Lippman-Young equation [12], which for an oil drop surrounded by water ambient is given by:

$$\theta(V) = \cos^{-1} \left[ \cos(\theta^o) - \frac{CV^2}{2\sigma_{wo}} \right] \quad [1]$$

where  $\theta^o$  is Young's angle (contact angle at 0 V),  $C$  is the capacitance per unit area of the dielectric stack covering the electrodes, which for this work consisted of two films, a 500-nm thick silicon dioxide and a 85-nm thick hydrophobic film,  $V$  is the applied voltage, and  $\sigma_{wo}$  is the surface tension between the water and oil phase.

Equation [1] was implemented as expressions for user defined variables, *thetaR* and *thetaL*, that are assigned as the contact angle for the left and right wetted-walls in the taper region. Voltages from zero to  $V_{max}$  were implemented through a solver parameter sweep and the equilibrium interface shape was solved for each new contact angle. Based on the dielectric materials used in this design,  $V_{max}$  was set at 40 V (see [8] for details). For each voltage value the total solution time was 1 ms. It was found that the liquid-liquid interface would reach equilibrium by that time. Automatic time stepping was done using the backward differentiation formulas (BDF) method, which is a default solver in COMSOL for this type of physics.

The liquid properties used in the simulations for the water and oil phases are listed in Table 1. The initial contact angle and surface tension were specified at  $\theta^o = 23^\circ$  and  $\sigma_{wo} = 45$  mN/m.

**Table 1 Liquid Properties**

Liquid	$\rho$ (kg/m <sup>3</sup> )	$\mu$ (Pa·s)	Index of Refraction
DI water	1000	$1 \times 10^{-3}$	1.33
Dodecane	750	$1.34 \times 10^{-3}$	1.421

#### 4.0 Simulation Results

Figure 3 shows contour plots of the liquid-liquid interface profiles for the same voltage values applied to each taper wall for a geometry of  $\alpha = 45^\circ$ ,  $h = 15$   $\mu\text{m}$ , and  $D_{ca} = 32$   $\mu\text{m}$ . The expression being plotted is the volume fraction of fluid 1, which is DI, with the contour level value set to 0.5.

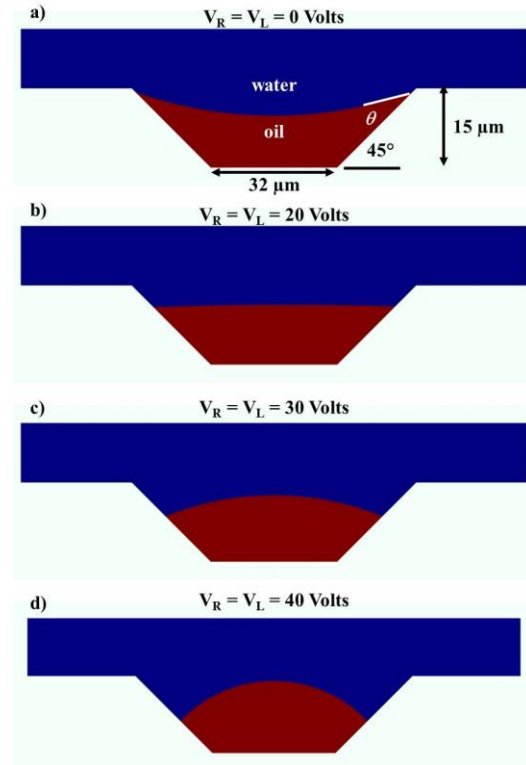


**Figure 3.** Contour plots of the liquid-liquid interface profile at different voltages for a microlens geometry of  $\alpha = 45^\circ$ ,  $h = 15$   $\mu\text{m}$ , and  $D_{ca} = 32$   $\mu\text{m}$ . a) Interface profile at 0 V. b) Interface profile at  $V_L = V_R = 20$  V. c) Interface profile at  $V_L = V_R = 30$  V. d) Interface profile at  $V_L = V_R = 40$  V.

For this voltage condition, the liquid lens will actively focus along the optical path, since the liquid lens profile stays centered in the taper cavity. The profile at 0 V for this taper angle and an initial contact angle of  $\theta = 23^\circ$  is concaved; this means the liquid microlens will have an initial negative optical power. The interface shape changes to convex at  $\sim 17$  V and the liquid microlens having positive optical power.

Since focusing and beam steering values will depend on the accuracy of the interface profile shape, i.e. the radius-of-curvature, it is important that the correct equilibrium contact angle as a function of voltage is being resolved. Figure 4 plots the contact angle vs. applied voltage for different automatically generated mesh sizes used for a liquid microlens geometry of  $\alpha = 45^\circ$ ,  $h = 15$   $\mu\text{m}$ , and  $D_{ca} = 32$   $\mu\text{m}$ . Figure 4 also includes the theoretical values based on Eq. [1].

To determine the resulting contact angle, the volume fraction (*vof*) of fluid 1 was exported to a data file and read into a MATLAB program, that

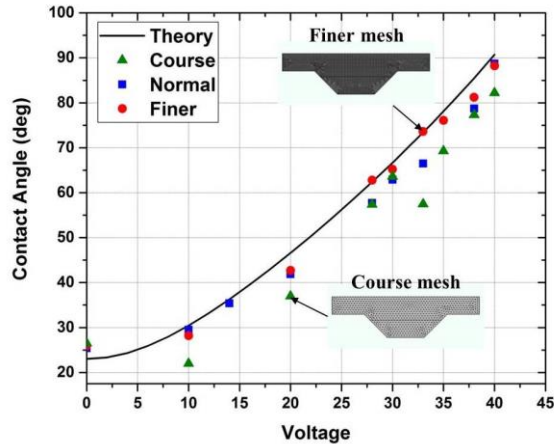


**Figure 4.** Contact angle vs. voltage for different automatically generated meshes for a microlens geometry of  $\alpha = 45^\circ$ ,  $h = 15 \mu\text{m}$ , and  $D_{ca} = 32 \mu\text{m}$ . The “coarse” mesh had 1,438 free triangular elements, the “normal” mesh 3,142 elements and the “finer” mesh 8,088 elements

determined the nodal position values for  $vof = 0.5$ . A polynomial fit of the position data was made and the contact angle was calculated using the fitted data.

Finite element meshes were generated under the User-Control setting, with free triangular elements. The element size was calibrated for fluid dynamics. Three mesh sizes were evaluated using predefined sizes – coarse, normal and finer. The *coarse* mesh had 1,438 elements, *normal* mesh 3,142 elements, and the *finer* mesh 8,088 elements. As the results show, the *coarse* and *normal* mesh sizes do not adequately resolve the equilibrium contact angle. The *finer* mesh resolved the equilibrium contact angle more accurately and was the mesh size setting used in all the simulation performed.

Several other taper angles were also evaluated. Figure 5 shows contour plots of the liquid-liquid interface profiles for the same voltage values applied to each taper wall for a geometry of  $\alpha = 15^\circ$ ,  $h = 15 \mu\text{m}$ , and  $D_{ca} = 32 \mu\text{m}$ . Figure 6 shows contour plots of the liquid-liquid interface profiles for the same voltage values applied to each taper wall for a geometry of  $\alpha = 75^\circ$ ,  $h = 15 \mu\text{m}$ , and  $D_{ca} = 32 \mu\text{m}$ .

As the results show, for a taper angle less than Young’s angle, the liquid-liquid profile will be convex at 0 V (Fig. 5a) and the liquid microlens will always have positive optical power. In the case when the taper angle is much greater than Young’s angle, approaching  $90^\circ$ , the liquid-liquid interface profile will become highly concaved. This means higher voltages are required before the liquid microlens has positive optical power, limiting the dynamic range, especially if there are limits to the maximum voltage that can be applied before dielectric failure.

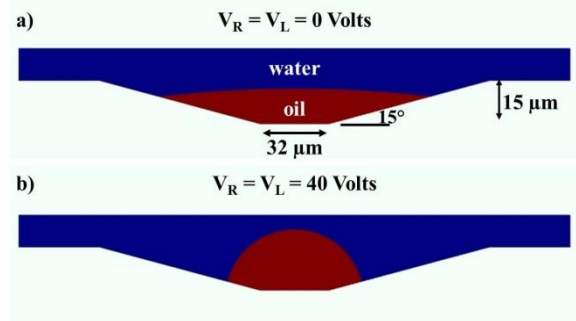


**Figure 5.** Contour plots of the liquid-liquid interface profiles at different voltages for a microlens geometry of  $\alpha = 15^\circ$ ,  $h = 15 \mu\text{m}$ , and  $D_{ca} = 32 \mu\text{m}$ . a) Interface profile at 0 V. b) Interface profile at  $V_L = V_R = 40 \text{ V}$ .

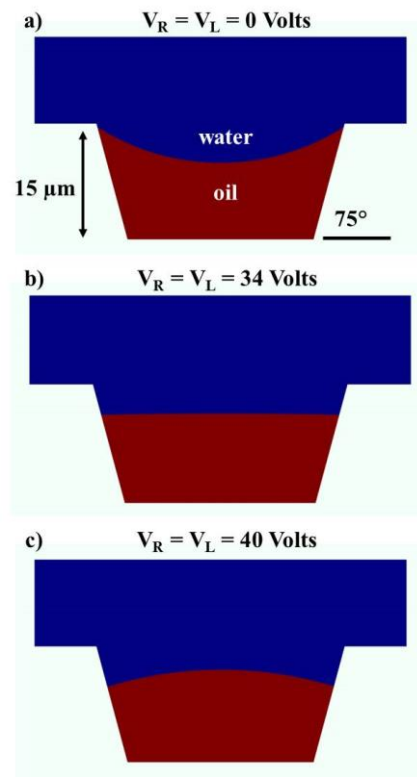


**Figure 6.** Contour plots of the liquid-liquid interface profiles at different voltages for a microlens geometry of  $\alpha = 75^\circ$ ,  $h = 15 \mu\text{m}$ , and  $D_{ca} = 32 \mu\text{m}$ . a) Interface profile at 0 V. b) Interface profile at  $V_L = V_R = 34 \text{ V}$ . c) Interface profile at  $V_L = V_R = 40 \text{ V}$ .

In the case of the  $75^\circ$  taper, the interface changes from concave to convex at  $\sim 34 \text{ V}$  compared to only  $\sim 17 \text{ V}$  for the  $45^\circ$  taper geometry.

#### 4.1 Focus Behavior

The parameters that influence focal length and the liquid interface curvature are 1) lens size, 2) liquids used to make up the lens, i.e. index of refraction

difference and 3) voltage through the electrowetting effect, i.e. surface tension and dielectric materials. In the results presented, the liquid microlens size was held constant with  $D_{ca} = 32 \mu\text{m}$ , and the liquid properties, with  $\Delta n = 0.09$ , in order to study trends in behavior with the taper angles.

The effect of the taper angle on focal range is shown in Fig. 7. The focal length is calculated by determining the radius-of-curvature from the liquid-liquid interface profile extracted from the *vof* data and using the Ray Transfer Matrix method. This approach not only calculates the focal length but will also calculate the beam steering angle. Details of the analysis are presented in Appendix B.

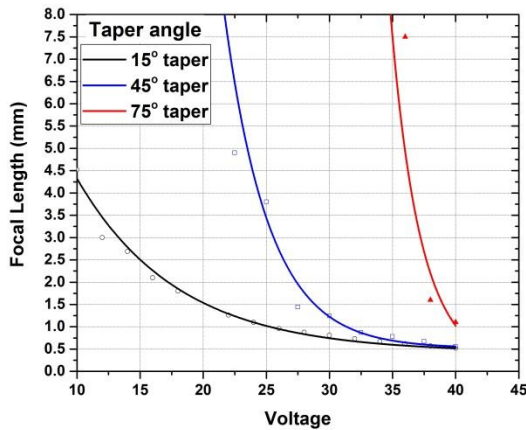


**Figure 7.** Estimated focus length vs. voltage for different cavity taper angles for geometries with  $h = 15 \mu\text{m}$ , and  $D_{ca} = 32 \mu\text{m}$ .

The results show the changes in focal length approaching a minimum limit. This is consistent with the radius-of-curvature getting smaller for increases in voltage and converging to a finite value. It is observed that once the contact angle of the interface on the sidewall becomes  $\geq 90^\circ$ , the focal length changes little with increases in voltage. The limit in focus will depend on the fluid properties:  $\Delta n$ , and  $\sigma_{wo}$ , as well as geometry, i.e. aperture size. For the liquids and the geometry modeled in these simulations, the minimum focal length is  $\sim 0.5 \text{ mm}$  at  $40 \text{ V}$ .

The results also show the steeper the taper angle, the smaller the dynamic range in the sense of operating voltage. In the case of  $\alpha = 75^\circ$ , the lens only has positive optical power over a very small voltage range, from  $34 \text{ V}$  to  $40 \text{ V}$  for this dielectric design, see Fig. 6. As a result, there are large changes in focal length for small increments in voltage. In practice, control of this type of electrowetting system can be difficult, especially if contact line pinning occurs [13].

## 4.2 Beam Steering

To steer a beam and simultaneously focus requires the curvature of the liquid microlens to maintain a spherical profile while being shifted. As described in Section 1.0 and [8], the liquid microlens can be shifted due to the geometry of the conical taper cavity and the ability to apply different voltages to different regions of the taper cavity, through interdigitated electrodes that are patterned along the taper sidewalls. To simulate the steering behavior in 2D, the liquid microlens model was created so different voltages could be applied to the left and right tapered sidewall.

Simulations were performed for a fixed voltage on the left side wall,  $V_L$ , and a voltage sweep on the right side wall, typically ranging from  $V_R = 20 \text{ V}$  to  $40 \text{ V}$ . The resulting interface profile for each voltage condition was then used to calculate the steering angle using the analysis in Appendix B.

Figure 8 shows an example of the contour plots for the liquid-liquid interface profiles for liquid microlens geometries having different taper angles for a voltage condition of  $V_L = 20 \text{ V}$ , and  $V_R = 40 \text{ V}$ .

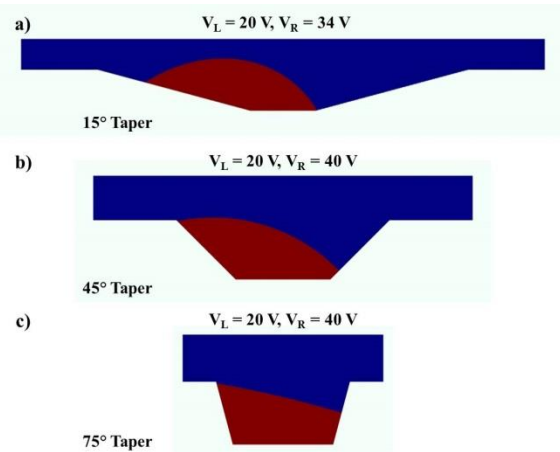


**Figure 8.** Contour plots of the liquid-liquid interface for different voltages applied to each taper sidewall, for geometries with  $h = 15 \mu\text{m}$ , and  $D_{ca} = 32 \mu\text{m}$ . a) Interface profile for  $15^\circ$  taper,  $V_L = 20 \text{ V}$ ,  $V_R = 34 \text{ V}$ . b) Interface profile for  $45^\circ$  taper,  $V_L = 20 \text{ V}$ ,  $V_R = 40 \text{ V}$ . c) Interface profile for  $75^\circ$  taper,  $V_L = 20 \text{ V}$ ,  $V_R = 40 \text{ V}$ .

The results show that as the taper angle approaches  $90^\circ$ , the liquid-liquid interface loses its curvature and becomes flat, much like a prism. This would be ideal if beam steering was the main goal. However, to be useful in optogenetics, the optic not only has to steer light but also focus light to a spot.

The relationship between steering angle and focus is captured in Fig. 9. The figure plots the estimated operational space of a liquid microlens for two different taper angles as indicated by the shaded area, bounded by steering angle and focus. In theory, the liquid microlens can be focused and a beam steered to any point within the shaded area. The data points in the plots are the results for simulated test cases, where  $V_L$  is held at a fixed voltage and a voltage range for  $V_R$  is applied.

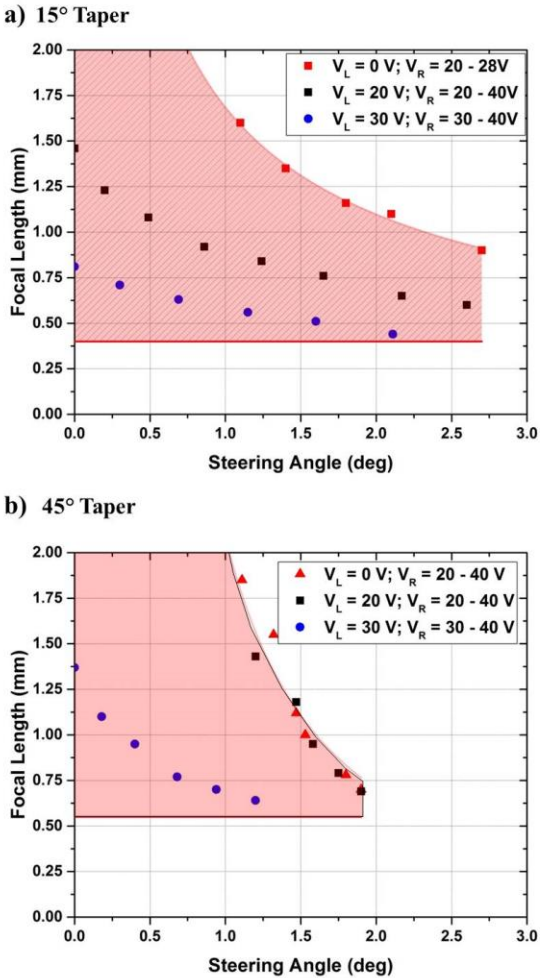


**Figure 9.** Focal length vs. steering angle for different  $V_L$  voltage conditions and voltage range applied to the opposite sidewall. a) Results for  $15^\circ$  taper with  $h = 15 \mu\text{m}$ , and  $D_{ca} = 32 \mu\text{m}$ . b) Results for  $45^\circ$  taper with  $h = 15 \mu\text{m}$ , and  $D_{ca} = 32 \mu\text{m}$ . Shaded area represents the operational space of the liquid microlens.

In Fig. 9a, the  $V_L = 0 \text{ V}$  condition represents the upper limit for the  $15^\circ$  taper design. This voltage condition would also be the upper limit for any taper angle less than Young's angle, since the liquid microlens will always have positive optical power for these cavity taper designs, and thus will focus and

steer for any voltage combination. The lower bound is shortest focus length that can be achieved at a maximum voltage of  $40 \text{ V}$ . For the  $15^\circ$  taper design, the shortest focus length  $f_{min} \cong 0.4 \text{ mm}$ . The maximum steering angle is  $\sim \pm 2.7^\circ$ . This translates into a focal spot shift from the optical axis of  $\pm 24 \mu\text{m}$  at a focus of  $500 \mu\text{m}$ .

In the case of the  $45^\circ$  taper, the upper limit is set by the voltage,  $V_{min}$ , which generates a contact angle equivalent to the taper angle. It was found that for the  $45^\circ$  taper design,  $V_{min} \cong 17 \text{ V}$ . Once this voltage is reached, the lens can now both simultaneously focus and beam steer. The lower bound for the operation space for the  $45^\circ$  taper design is  $f_{min} \cong 0.5 \text{ mm}$ . The maximum steering angle is  $\sim \pm 1.9^\circ$ . This translates into a focal spot shift from the optical axis of  $\pm 17 \mu\text{m}$  at a focus of  $500 \mu\text{m}$ .

## 5.0 Simulation vs. Experimental Results

Based on the simulation results, several different liquid microlens geometries were chosen to be fabricated that could potentially reach our design criteria. Because of practical microfabrication issues, creating a deep, shallow taper angle is very challenging. Therefore, initial liquid lenses were fabricated and evaluated with a  $15 \mu\text{m}$  deep,  $45^\circ$  conical taper [8].

Figure 10 shows an example of focal length as a function of voltage for liquid microlenses of different clear aperture sizes. Included are the predicted focal length values from numerical simulations.

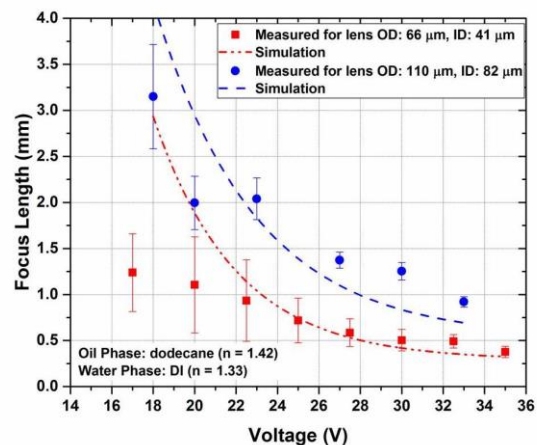


**Figure 10.** Measured and predicted focal length vs. voltage for different sized lenses. Error bars represent standard deviation from the data set. Reprinted from [8] with permission.

The measured and predicted focal length measurements show good agreement, especially at higher voltages when the contact angle changes are

large per increases in voltage and the system is less sensitive to small variations to contact angle and the liquid microlens radius-of-curvature.

The steering angle was measured for several lenses, but with a limited data set. Figure 11 compares the measured steering angle to the predicted steering angles for a liquid lens size of  $D_{ca} = 82 \mu\text{m}$ ,  $h = 12 \mu\text{m}$  and  $\alpha = 48^\circ$ . In this test case,  $V_L = 20 \text{ V}$  and  $V_R = 30 \text{ V}$  and  $35 \text{ V}$ . The absolute values from the simulation results did not match the measured steering angle. There could be several reasons for this, both from the modeling assumptions and fabrication/testing issues. However, the trend in the steering angle behavior with applied voltage does agree between simulation and measurements.

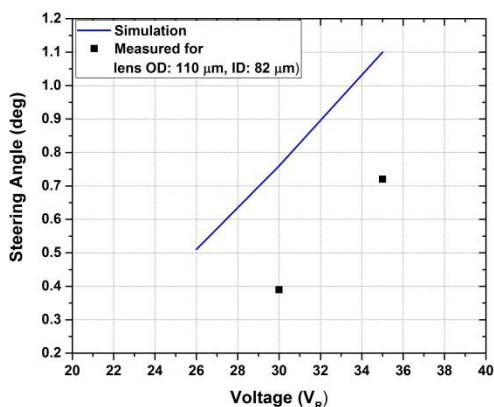


**Figure 11.** Measured vs. predicted steering angle vs. voltage for a geometry of  $\alpha = 48^\circ$ ,  $h = 12 \mu\text{m}$ , and  $D_{ca} = 82 \mu\text{m}$ , with  $V_L = 20 \text{ V}$ .

## 6.0 Conclusions

Two-dimensional numerical simulations were performed to study the liquid-liquid interface profile behavior in a liquid microlens controlled by electrowetting. The level-set method was used to model the two liquid phases and shown to provide accurate results. It should be noted that equivalent analytical models could have been derived, however using numerical simulations allowed for rapid assessment and visualization of different geometry configuration.

The results indicated that having a taper angle less than Young's angle for a given liquid-liquid-solid system, would be the best design for a liquid lens that is supposed to simultaneously focus and steer. However, there is a tradeoff between what can be microfabricated and taper angle.

One limitation of this modeling work was not being able to look at the liquid microlens quality, such as spherical aberrations, coma, astigmatism, etc.

especially for the beam steering cases, since only 2D simulations were performed. A 3D model would be able to capture many of the liquid lens quality attributes. Based on this work, the foundation for creating a three-dimensional (3D) model using the level-set method is in place.

## References

1. K. Deisseroth, G. Feng, A. Majewska, G. Miesenbröck, A. Ting, and M. Schnitzer, "Next-Generation Optical Technologies for Illuminating Genetically Targeted Brain Circuits," *J. Neurosci.*, **26**(41), 10380 (2006).
2. E. Boyden, F. Zhang, E. Bamberg, G. Nagel, and K. Deisseroth, "Millisecond-timescale, genetically targeted optical control of neural activity," *Nature Neuroscience*, **8**(9), 1263-1268 (2005).
3. N. C. Klapoetke, Y. Murata, S. S. Kim, S. R. Pulver, A. Birdsey-Benson, Y. K. Cho, T. K. Morimoto, A. S. Chuong, E. J. Carpenter, Z. Tian, J. Wang, Y. Xie, Z. Yan, Y. Zhang, B.Y. Chow, B. Surek, M. Melkonian, V. Jayaraman, M. Constantine-Paton, G. K. Wong, and E. S. Boyden, "Independent Optical Excitation of Distinct Neural Populations," *Nature Methods*, **11**, 338-346 (2014).
4. F. Mugele, and J. Baret, "Electrowetting: from basics to applications," *J. Phys.: Condens. Matter*, **17**, R705-R774 (2005).
5. S. Kupier and B. H. W. Hendriks, "Variable-focus liquid lens for miniature cameras," *Appl. Phys. Lett.*, **85**(7), 1128-1130 (2004).
6. B. Berge and J. Peseux, "Variable focus lens controlled by an external voltage: An application of electrowetting," *Eur. Phys. J.*, **E3**(2), 159-163 (2000).
7. D. Kopp, T. Brender, and H. Zappe, "All-liquid dual-lens optofluidic zoom system," *Appl. Opt.*, **56**(13), 3758-3763 (2017).
8. S. Berry, S. Redmond, P. Robinson, T. Thorsen, M. Rothschild, and E. S. Boyden, "Fluidic microoptics with adjustable focusing and beam steering for single cell optogenetics," *Optics Express*, **25**(14), 16825-16839 (2017).
9. E. Olsson, and G. Kreiss, "A conservative level set method for two phase flow," *J. Comput. Physics*, **210**, 225-246 (2005).
10. "Inkjet Nozzle – Level Set Method," Application Library, COMSOL Multiphysics, [www.comsol.com](http://www.comsol.com).
11. "The Level Set Interface," Chapter 10: Mathematics, User Manual, COMSOL Multiphysics, [www.comsol.com](http://www.comsol.com).
12. M. Mailard, J. Legrand, and B. Berge, "Two liquids wetting and low hysteresis electrowetting on dielectric applications," *Langmuir*, **25**(11), 6162-6167 (2009).

13. F. Li and F. Mugele, “How to make sticky surfaces slippery: Contact angle hysteresis in electrowetting with alternating voltage,” *Appl. Phys. Lett.*, **92**(24), 244108 (2008).

### **Acknowledgements**

This material is based upon work supported by MIT under Air Force Contract No. FA8721-05-C-0002 and/or FA8702-15-D-0001. Any opinions, findings, conclusions or recommendations expressed in this material are those of the author(s) and do not necessarily reflect the views of MIT.

## Appendix A: Level-Set Method

In this method, the fluid-fluid interface moves with fluid velocity  $\mathbf{u}$ . The flowing transport equation describes the convection of the level-set function:

$$\frac{d\phi}{dt} + \nabla \cdot (\phi \mathbf{u}) + \gamma \left[ \left( \nabla \cdot \left( \phi(1-\phi) \frac{\nabla \phi}{|\nabla \phi|} \right) \right) - \varepsilon \nabla \cdot \nabla \phi \right] = 0 \quad [1]$$

The thickness of the transition layer is proportional to  $\varepsilon$  which typically defaults to half the maximum element size in the model. The parameter  $\gamma$  determines amount of reinitialization and is set to magnitude of the velocity field. It should be noted that static equilibrium shapes are being determined for the liquid microlens, meaning the velocity field will be zero. Thus,  $\gamma$  was set to the default value of 1.0 for this modeling work. As will be demonstrated, a surface tension surface term included in the momentum equation will couple with the level-set contour function.

The fluid flow is defined with the mass and momentum equations. In the case of the liquid microlenses, both the water and oil phases can be considered incompressible leading to the following Navier-Stokes equations:

$$\rho \left( \frac{\partial \mathbf{u}}{\partial t} + \mathbf{u} \cdot \nabla \mathbf{u} \right) - \nabla \cdot (\mu (\nabla \mathbf{u} + \nabla \mathbf{u}^T)) + \nabla p = \mathbf{F}_{st} \quad [2]$$

$$(\nabla \cdot \mathbf{u}) = 0 \quad [3]$$

$\mathbf{F}_{st}$  is a volumetric source term, which for two-phase flow is the surface tension force at the fluid-fluid interface. The surface tension is computed as:

$$\mathbf{F}_{st} = \nabla \cdot \mathbf{T} \quad [4]$$

$$\mathbf{T} = \sigma (\mathbf{I} - (\mathbf{n}\mathbf{n}^T)) \delta \quad [5]$$

where  $\mathbf{I}$  is the identity matrix,  $\mathbf{n}$  is the interface normal,  $\sigma$  is the surface tension, and  $\delta$  equals a Dirac delta function. The normal to the fluid-fluid interface is found using the level set contour function:

$$\mathbf{n} = \frac{\nabla \phi}{|\nabla \phi|} \quad [6]$$

Not only will the fluid-fluid interface be influenced by the velocity field but also by surface tension.

## Appendix B: Focus and Beam Steering Analysis

Using the Ray Transfer Matrix method the focal length and beam steering angles are determined from the liquid-liquid interface profile. The volume fraction (*vof*) of fluid 1 is exported to a data file and read into a MATLAB program that determines the nodal position values for *vof* = 0.5. A polynomial fit of the position data is then made that generates a well-defined interface profile. From the interface profile, the equilibrium contact angle,  $\theta$  and width of the profile shape,  $C$ , are determined. The in-plane radius-of-curvature,  $R$  can be calculated from:

$$R = \frac{C}{2 \sin(\theta)} \quad [1]$$

For the liquid microlens the analytical model used for ray tracing is shown in Fig. 1.

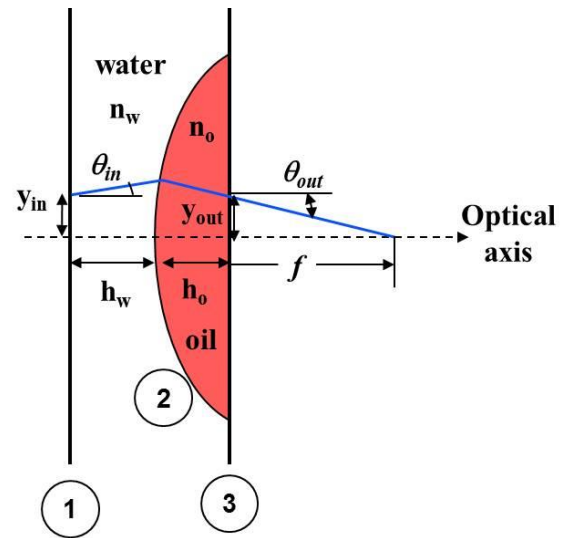


**Figure 1.** Geometry for the optical layout of the liquid microlens and the location of input and output planes.

The expression describing a ray propagating through the input and output planes of the liquid microlens geometry is given by:

$$\begin{bmatrix} y_{out} \\ \theta_{out} \end{bmatrix} = [\mathbf{M}] \begin{bmatrix} y_{in} \\ \theta_{in} \end{bmatrix} \quad [2]$$

where  $[\mathbf{M}]$  is the ray transfer matrix and is defined at each interface in the optical path as  $[\mathbf{M}] = \mathbf{M1} \cdot \mathbf{M2} \cdot \mathbf{M3}$  where:

$$\mathbf{M1} = \begin{bmatrix} 1 & h_w \\ 0 & 1 \end{bmatrix} \quad [3a]$$

$$\mathbf{M2} = \begin{bmatrix} 1 & 0 \\ \frac{n_w - n_o}{Rn_o} & \frac{n_w}{n_o} \end{bmatrix} \quad [3b]$$

$$\mathbf{M3} = \begin{bmatrix} 1 & h_o \\ 0 & 1 \end{bmatrix} \quad [3c]$$

where  $h_w$  is the water thickness,  $h_o$  is the height of the liquid lens measured from liquid-liquid interface contact location in the taper,  $n_w$  is refractive index of the water phase,  $n_o$  is the refractive index of the oil phase, and  $R$  is the radius-of-curvature.

The same method was used to find the steering angle. When the interface shifts in the tapered cavity, the apex of the interface curvature no longer aligns with optical axis of the lens, as shown in Fig. 2. The distance from the apex to the original optical axis is determined and used as the  $y_{in}$  value.  $\theta_{in}$  is set at  $0^\circ$ . From eq. [2], the steering angle  $\alpha$  is then equal to  $\theta_{out}$ .

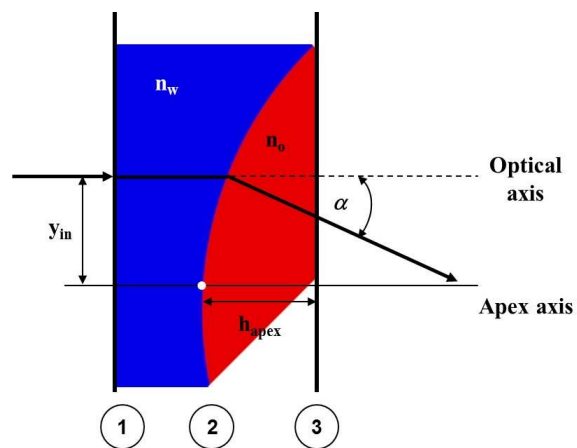


**Figure 2.** Geometry used to determine the steering angle of a tilted liquid microlens.